Acta Crystallographica Section A
Foundations of Crystallography
ISSN 0108-7673

Received 3 February 2004
Accepted 2 August 2004

Shadowing and absorption corrections of high-pressure powder diffraction data: toward accurate electron-density determinations

Andrzej Katrusiak

Faculty of Chemistry, Adam Mickiewicz University, Grunwaldzka 6, 60-780 Poznań, Poland.
Correspondence e-mail: katran@amu.edu.pl

The shadowing of the primary beam and of reflections from a powder crystal sample enclosed in a diamond-anvil high-pressure cell (DAC) is described for unrestricted data-collection procedures. The corrections account for the shadowing of the data measured with point- or area-detector diffractometers and can be applied for any containers of environment devices enclosing a powdered sample. The general procedure for correcting the powder diffraction data can be applied for analysing and optimizing diffractometric procedures of data collection and provides facilities for collecting high-pressure powder diffraction data with the DAC positioned optimally and rotated to counteract the preferred-orientation and particle-size effects, and to increase the resolution of data. The quadrature effects of numerical integration for the accuracy of computed corrections have been analysed.

1. Introduction

Powder diffraction is one of the most powerful analytical methods, increasingly often applied for structural determinations. It has been demonstrated that high-quality structural results can be obtained for mixtures of polymorphs (Dinnebier *et al.*, 1997), or even for powdered protein crystals (Von Dreele, 1999, 2001; Von Dreele *et al.*, 2000). Powder diffraction is particularly useful in the field of structural transformations, when single crystals are difficult to obtain at extreme conditions or become damaged at phase transitions (McMahon, 2004; Parise, 2004; Crichton & Mezouar, 2004). Structural transformations are efficiently generated by elevated pressures. This fact may considerably hamper investigations of electron-charge density or even structural investigations at high pressures by single-crystal diffraction: on the one hand, one would be interested in generating high pressures to induce appreciable effects in the charge density and, on the other hand, most substances will transform at high pressures to another phase and the transition is likely to damage single-crystalline samples. Moreover, any transformations in electron-charge density modifies the pattern of interatomic, intermolecular or interionic interactions, which are responsible for the crystal structure of materials. Consequently, those substances in which high pressures induce electron-density transformations are likely to undergo structural phase transitions. A possible method to overcome this difficulty is to crystallize a single crystal *in situ* at elevated pressure. It requires that the sample be heated and melted at high pressure. In many cases, the pressure crystallization naturally leads to a nice single crystal, especially for pressures of up to a few GPa. However, in certain cases, it may be difficult to obtain a single crystal. For most substances, the melting point rises considerably with pressure, and the sample may decompose before its melting temperature is reached. In some cases, the phases of interest may have no interphase boundaries with the liquid state and the *in situ* crystallization leading to a single crystal may be impossible. Some substances may be simply 'reluctant' to form single crystals, even at ambient conditions, and a powder diffraction measurement may be the only resort to obtain the structural information.

Meanwhile, electron-charge density and time-resolved structural determinations appear as ultimate goals of accurate high-pressure diffraction studies. At present, the charge density in crystals is determined mainly at low temperatures – usually around and below 100 K – and for substances with a varied chemical composition. Thus, of two fundamental thermodynamic variables, temperature and pressure, only the temperature can be routinely adjusted in a limited range. Pressure-induced transformations of the charge density are needed for a fuller functional understanding of atomic, molecular and supramolecular properties (Nicol & Yin, 1981). In general, electron-density and structural studies at extreme conditions are essential for the development of comprehensive chemistry and physics, which would include *e.g.* the phenomena in the interiors of the Earth and other celestial planets.

It was evidenced, mainly through observations of changing physical properties, that elevated pressure can induce dramatic transformations in the electronic structure of substances. Among the most eminent examples are transformations between different crystal types of phosphorus

(Kikegawa & Iwasaki, 1983) and praseodymium (Baer *et al.*, 2003), pairing of atoms in lithium (Neaton & Ashcroft, 1999), insulator–metal phase transitions (Siringo *et al.*, 1990; Mesot *et al.*, 1995; Adler *et al.*, 1999), metallization of oxygen (Akahama *et al.*, 1995; Serra *et al.*, 1998), xenon (Chacham *et al.*, 1992; Eremets *et al.*, 2000), hydrogen (Edwards & Hensel, 1997), superconductivity of elements (Struzhkin *et al.*, 1997; Hemley, 1998; Shimizu *et al.*, 1998), semiconducting non-molecular nitrogen phase (Goncharov *et al.*, 2000; Eremets *et al.*, 2001), and other types of transformations evidenced in elements or simple compounds. However, practically an unlimited variety of transformations related to charge density can be predicted in the realm of organic substances. Investigations of charge density in organic or complex compounds would contribute considerably to the understanding of the most fundamental concepts of chemistry and biology.

Electron-density determinations at high pressures can be performed by either single-crystal or powder diffraction analysis. Although in specific cases diffraction intensity of specific extinguished reflections can be considered as a marker of undergoing electron-density transformations in simple systems (Yoder-Short *et al.*, 1982; Yin & Cohen, 1983), the precise electron distribution can be revealed only through the highest possible accuracy and completeness to a high resolution of the measured data. These requirements have been partly fulfilled by the significant technological advances in the field of high-pressure powder diffraction techniques, marked by the inception of electronic area detectors and their application to high-pressure studies at the end of the 1980's (Fujii *et al.*, 1989; Meade & Jeanloz, 1990) and increasingly common application of synchrotron radiation (Prewitt *et al.*, 1987; Coppens *et al.*, 1992; Piltz *et al.*, 1992; Nelmes *et al.*, 1992; Shimomura *et al.*, 1992). Studies with the diamond-anvil cell (DAC) and synchrotron radiation were soon successfully perfected and applied to solving numerous pressure-induced structural transformations. The single-crystal experiments are better than the powder ones where the precision is concerned, and this method was chosen for the first studies of electron density at high pressures (Shobu *et al.*, 2001).

High-pressure crystallography is usually associated with experimental limitations due to relatively large vessels enclosing much smaller samples. Thus a number of corrections of the measured data is required for the effects due to the high-pressure experimental set. The most significant effects include, apart from the DAC and sample absorption, also the shadowing of the sample by the gasket edges or the preferred orientation of crystallites in the compressed powder. The purpose of this work is to report a general way of correcting shadowing and absorption effects for powder diffraction experiments – a new configurational type of the contribution to these effects considerably improves the precision of the reflection-intensity measurements. The general approach to the shadowing corrections can also be applied for minimizing and evaluating the preferred-orientation or finite-particle-size effects.

Of thermodynamical variables, it is undoubtedly temperature that has been changed most often for structural studies, however during recent decades pressure changes have also been increasingly applied (Hazen & Finger, 1982). For performing experiments at varied thermodynamical conditions, environment containers are usually used: furnaces, cryostats and glass or metal capillaries. In the case of high-pressure diffraction structural experiments, the absorption and shadowing of the DAC is particularly significant and reflection intensities require obligatory corrections for obtaining structural results (Merrill & Bassett, 1974). Most recently, we have described the absorption and gasket-shadowing corrections for a DAC and single-crystal sample treated together as a composite absorber of X-rays. This general vector approach revealed new beams–DAC configurational features of the gasket shadowing effect. The effect of configurational contributions to gasket shadowing will now be described for powder crystalline samples. It will be shown that the magnitudes of absorption and shadowing effects are key factors for planning the optimum mode of collecting intensity data and even for avoiding systematic errors in measuring Bragg diffraction angles.

2. Methodology

High-pressure diffraction experiments on powders in certain respects resemble those on single-crystal samples of pressure-frozen liquids or gases in that the powder sample usually fully fills the high-pressure chamber (Von Dreele & Hanson, 1984). For this reason, the shadowing effect is particularly significant for the structural analysis of powders. Also, the increasingly common application of area detectors, image plates or CCD detectors (Chall *et al.*, 2000; Allan *et al.*, 2002; Budzianowski & Katrusiak, 2004), as well as new powerful X-ray sources and highly efficient optical devices for beam collimation in X-ray laboratories (Katrusiak, 2004*a*), set new standards for powder

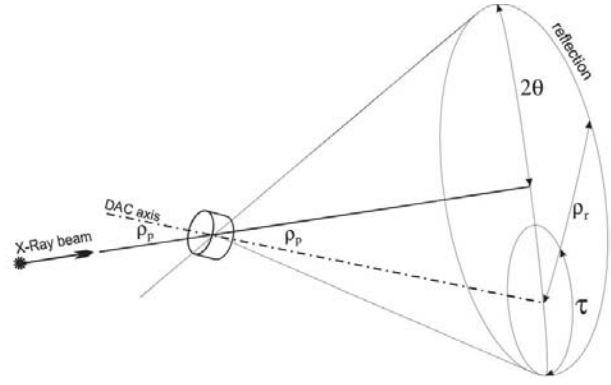

Figure 1
Schematic representation of one reflection cone diffracted from a powdered sample contained in a cylindrical chamber. The DAC axis is represented by the dot-and-dash line, and the angle between the primary beam and the chamber axis is denoted ρ_p; the angle between the reflected beams within each powder reflection, denoted ρ_r, depends on the mutual arrangement of the primary beam, the DAC axis and the reflected beam, measured by torsional angle τ of the beams about the DAC axis. For the sake of clarity, only one reflection cone has been shown. It is unusual in experimental practice that the small volume of the DAC chamber contains enough powder grains to produce a continuous reflection ring (*cf.* Fig. 2).

diffraction experiments: smaller sample volumes and more sophisticated environment attachments are now possible. The geometrical modes of data collection are of straightforward significance for data reduction. Meanwhile, a numerical procedure correcting the absorption and shadowing affecting single-crystal intensities measured in a general data-collection mode has been described only recently (Katrusiak, 2004*b*). Now this concept will be applied to powder diffraction experiments.

In the discussion below, the Eulerian-cradle terminology, commonly applied for normal-beam equatorial four-circle diffractometers, will be used. The environmental attachment chambers are usually confined to small volumes, and parallel-beam or nearly parallel beam techniques are favoured over Bragg–Brentano divergent-beam methods. Therefore, the shadowing and absorption effects will be discussed for parallel or weakly divergent beams from laboratory X-ray sources (Katrusiak & Ryan, 1988). This can be extended to the methods with non-parallel beams by convoluting the results with the beam divergence.

A schematic diagram of the experimental set-up is shown in Fig. 1. We shall assume that the powdered sample fully fills the chamber of cylindrical symmetry. This is the most common case in high-pressure powder diffraction experiments, and also in the case of single crystals of pressure-frozen gases and liquids (Von Dreele & Hanson, 1984; Allan *et al.*, 2002; Katrusiak, 2004*b*; Bujak *et al.*, 2004). When the sample and the environmental device are treated generally as a composite absorber, the effects termed shadowing and absorption cannot be clearly discriminated: the absorption of all elements of the DAC different from the sample, which weaken either the incident beam or the reflection, can be treated as a partial shadowing effect; the term shadowing will not be applied to the absorption of the sample itself, even though one can argue that the sample parts are partly shadowed by other parts on the way either to the collimator or to the detector. Thus, generally, the discussion can be limited to the effect of absorption. However, because of the strong absorption of the gasket, it is convenient to assume that it is totally opaque to X-rays – this allows the calculations to be performed only for those portions of the sample that are illuminated by the primary beam and reflections of which are not obscured by the gasket.

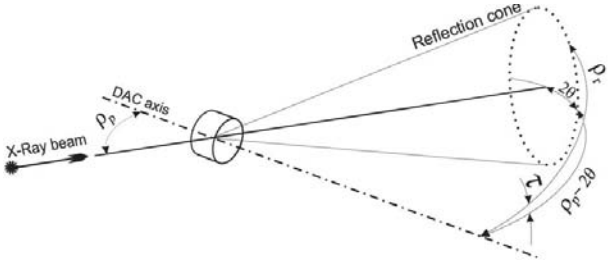

Figure 2
One powder reflection ring of the cylindrical sample when Bragg angle 2θ is smaller than the inclination angle of the primary beam to the axis of the cylindrical DAC chamber, ρ_p. The symbols used in Fig. 1 have been applied but the reflection ring has been drawn with a dotted line, which would correspond to fewer crystal grains in this powder sample.

The nomenclature introduced for the analysis of shadowing and absorption effects in single-crystal diffraction experiments (Katrusiak, 2001, 2004*b*) will be applied. The same technique of numerical integration will be used for calculating the beam intensity illuminating a sample portion and the transmission of the reflection leaving the DAC. All the calculations will be performed in the φ-axis reference system. Of the Eulerian cradle, only the ω axis will be used for rotating the DAC, which is consistent with the operation of typical powder diffractometers. Then the versor along the primary beam, $\mathbf{v}_p$, expressed in the φ-axis system is

$$\mathbf{v}_p = R_\omega \begin{pmatrix} -1 \\ 0 \\ 0 \end{pmatrix}. \tag{1}$$

The DAC cylindrical-symmetry vector $\mathbf{v}_{\rm DAC}$ is

$$\mathbf{v}_{\rm DAC} = \begin{pmatrix} 1 \\ 0 \\ 0 \end{pmatrix}. \tag{2}$$

The powder scattering vectors lie along the cone with the vertex at the sample and the opening angle about the primary beam of 2θ (see Figs. 1 and 2). In matrix notation, the powder reflection vectors $\mathbf{v_r}$ can be expressed as

$$\mathbf{v_r}(\zeta) = \mathbf{R}_{-\omega}\mathbf{R}_\zeta\mathbf{R}_{2\theta}\begin{pmatrix} -1 \\ 0 \\ 0 \end{pmatrix}, \tag{3}$$

where

$$\mathbf{R}_\omega = \begin{pmatrix} \cos\omega & \sin\omega & 0 \\ -\sin\omega & \cos\omega & 0 \\ 0 & 0 & 1 \end{pmatrix},$$

$$\mathbf{R}_{2\theta} = \begin{pmatrix} \cos 2\theta & \sin 2\theta & 0 \\ -\sin 2\theta & \cos 2\theta & 0 \\ 0 & 0 & 1 \end{pmatrix},$$

$$\mathbf{R}_\zeta = \begin{pmatrix} 1 & 0 & 0 \\ 0 & \cos\zeta & \sin\zeta \\ 0 & -\sin\zeta & \cos\zeta \end{pmatrix}$$

are rotation matrices; angle ω is the vertical goniometer shaft off-setting the DAC axis from the primary beam (thus angles $|\omega|$ and ρ_p are equivalent when the sample is not rotated about axis φ), θ is the Bragg angle of a given reflection and ζ is the angle of rotation about the primary beam. For an ideally homogeneous non-polarized primary beam and a small, spherical and ideally powdered sample without any containers or mounting devices, the intensity distribution around the reflection ring should be constant.

3. Synchrotron microbeams

Several effects should be considered when measuring a typical reflection from a powder sample enclosed in a DAC. First, a

series of example beams–DAC arrangements will be considered for a parallel microbeam – which is commonly used at synchrotron sources (Fiquet & Andrault, 1999). It is ideal when none of the registered reflections is obscured by the gasket – the situation illustrated in Fig. 3(*a*). The higher-2θ angle reflections can be partly shadowed by the gasket edges (Fig. 3*b*). The correction of the intensity of the reflections due to the shadowing of the ideally centred microbeam (with the beam diameter much smaller than the diameter of the high-pressure chamber) can be derived from the volume of the sample illuminated by the beam and not shadowed in the reflection direction from the detector side:

$$V_s = \begin{cases} HS & \text{for } \tan(2\theta) \le D/2H \\ DS/[2\tan(2\theta)] & \text{for } \tan(2\theta) > D/2H, \end{cases} \quad (4)$$

where H and D are the height and diameter of the high-pressure chamber, and S is the cross-section surface of the primary beam.

This shadowing can be eliminated in part of the powder reflection ring by tilting the DAC axis to the primary beam, which however is obtained at the cost of increased shadowing in the trans-annular portions of the ring (Fig. 3*c*). The tilting of the DAC axis by angle ω increases the volume of the sample powder illuminated by the primary beam, which increases the reflection intensity by the factor

$$t_\rho = 1/\sin\rho_p. \quad (5)$$

In this respect, the DAC tilting increases the efficiency of measurements. However, the shadowing can be fully eliminated in part of the reflection ring only when the Bragg angle

$$\theta > D/(2H). \quad (6)$$

The sample shadowing can be avoided only for low-angle reflections – fulfilling the first of the criteria in (4) for the DAC aligned along the primary beam. For measuring more reflections, either shorter wavelengths (Crichton & Mezouar, 2004) or wider DAC windows are required. The higher-angle reflections are shadowed and introduce errors into the measurements of the unit-cell dimensions, profiles of the reflections and their intensities.

Thus the DAC tilting may considerably increase intensities in parts of the reflection rings. But, more importantly, the DAC tilting is the only means of measuring these reflections, for which angle 2θ is larger than the maximum opening angle of the DAC (measured relative to the DAC axis). For example, for the NaCl sample and Mo $K\alpha$ radiation, only the ten lowest θ-angle reflections to a resolution of 1.039 Å can be recorded for the DAC with the standard window opening half-angles of 40°, when the DAC is positioned at $\omega = 0°$. By tilting the same DAC to $\omega = 40°$, the resolution of the accessible diffraction data becomes 0.553 Å and the number of accessible reflections considerably increases to 49 (the systematically extinguished reflections have not been counted).

The effect of absorption and shadowing on the reflections of narrow microbeams for an inclined sample can be easily derived from analytical trigonometric considerations or numerically. The numerical method has the advantage of convenient implementation of various factors – absorption, extinction, various shapes of the high-pressure chamber, gasket-material absorption, extended dimensions of the beam *etc*., without considerable complication of the procedure. Therefore, the numerical method has been applied in this paper.

Despite the apparent advantages of powerful synchrotron microbeams, their drawbacks arise from the small volume of illuminated sample and of the limited number of diffracting grains of the investigated powder.

4. Laboratory sealed-tube sources

It is characteristic of conventional sealed X-ray tubes, commonly applied in laboratories, that the diameter of the primary beam is larger than the size of the high-pressure chamber. Single crystals investigated in laboratories have dimensions of a few tenths of a millimetre and should be fully bathed in the beam. For the high-pressure studies, the broad primary beam has the advantage of the increased sample volume actively contributing to the reflection intensity, as shown in Fig. 4, and therefore involving more powder particles in the diffraction events. Sealed-tube beams have much lower intensity compared to synchrotron beams, which is very disadvantageous for the counting statistics, but in certain cases can be required for avoiding structural changes induced in the crystal by the beam. For the samples fully filling the high-pressure chamber and illuminated by a broad beam, the shadowing effect is prominent. However, the shadowing can

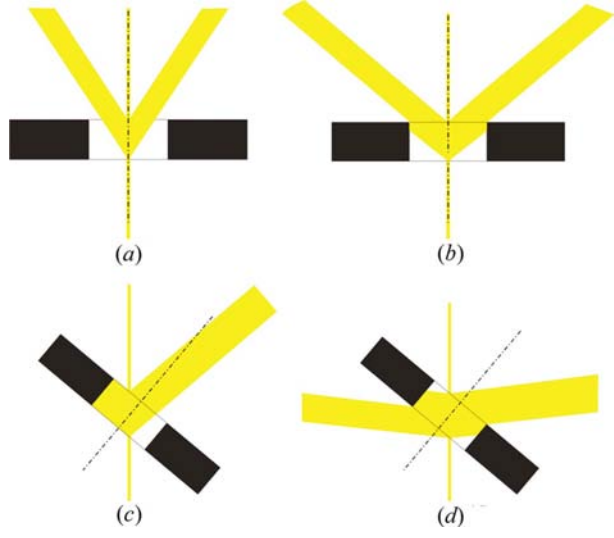

Figure 3
Several example cross sections through one powder reflection ring obtained from a micro primary beam and the DAC at various orientations. The sections show the high-pressure chamber (gasket is shown in black) and the reflection ring (primary and reflected beams are shaded) in the ω–2θ plane: (*a*) the DAC axis is collinear with the primary beam, and the reflection not obscured by the gasket; (*b*) the primary beam is collinear with the DAC but the reflection is partly shadowed by the gasket; (*c*) the same reflection as in the previous drawing, but the DAC axis is inclined to the primary beam by angle $\omega = \rho_p = 90° - 2\theta$; and (*d*) a higher 2$\theta$ angle reflection than in (*c*) and the same DAC inclination angle, ρ_p.

be straightforwardly corrected by the numerical method (Busing & Levy, 1957; Burnham, 1966; Katrusiak, 2004*b*). Fig. 4 shows a section through the DAC chamber and the powder reflection ring diffracted at Bragg reflection angle 2θ of 50°. The opening angle of most Merrill–Bassett DAC's is about 40°, thus the refection in Fig. 4(*a*) could not be recorded for the DAC positioned at ω equal to 0°. If the DAC is tilted to angle ω equal to 30°, the inclination of the DAC axis to the reflection ring on one side is reduced to

$$\rho_r(\text{min}) = 2\theta - \omega \tag{7}$$

and on the other side of the reflection ring it is increased to

$$\rho_r(\text{max}) = 2\theta + \omega. \tag{8}$$

Equations (7) and (8) are valid when $2\theta > \omega$. For the low-angle reflections with $2\theta < \omega$, equation (8) remains valid (see Fig. 2) but

$$\rho_r(\text{min}) = \omega - 2\theta. \tag{9}$$

Figure 4
Sections through the high-pressure chamber illuminated with a broad primary beam and the same reflection ring for two orientations of the DAC: (*a*) the DAC axis aligned along the primary beam; and (*b*) the DAC axis off-set from the primary beam by 30°. The sample portions contributing to the sections of reflection rings are different depending on the angles θ and ζ, and on the orientation of the DAC. In these cross sections, the parts of the sample that diffract to the right part of the reflection ring (ζ = 0°, *cf.* Figs. 1 and 2) are shown in red.

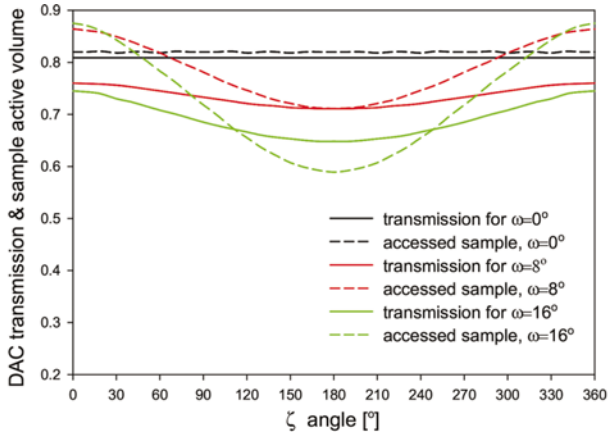

Figure 5
Relative transmission of a typical Merrill–Bassett DAC (referred to the transmission of the primary beam passing along the DAC axis) and the relative sample volume actively contributing to the reflection for a reflection ring with the Bragg angle 2θ of 30°, and various values of ω (DAC inclination to the primary beam) equal to 0, 8 and 16°, plotted against the ζ angle (see text).

Angles ρ_r outside the ω plane (see Figs. 1 and 2) can be straightforwardly calculated from the scalar and vector products of vectors $\mathbf{v}_{\text{DAC}}$ and $\mathbf{v}_{\mathbf{r}}$.

The DAC transmission and the sample active volumes calculated for a powder reflection at θ = 15° at various ω angles are shown in Fig. 5. In this and in later analogous plots, the DAC transmission for $\rho_p = \rho_r = 0°$ has been normalized to 1.0, and it has been assumed that the transmissions of the two DAC halves are equal. The true transmission of a typical Merrill–Bassett DAC anvil at $\rho_p = \rho_r = 0°$ is *ca* 0.7, thus the relative transmissions should be multiplied by 0.5 to obtain the true magnitude of the transmission. For the angle ζ equal to 0°, the relative magnitudes of the DAC transmission and sample active volume are 0.809 and 0.820, respectively. Thus, the combined effect reducing the beam intensity is 0.663. When ω is increased to 8°, the DAC transmission decreases to 0.760 and the active sample volume increases to 0.864, giving a slight decrease in the combined intensity reduction to 0.657. When ω is further increased to 16°, the DAC transmission decreases only slightly to 0.745, the active sample volume increases to 0.875 and the combined intensity reduces to 0.652. The favourable combined effect of the DAC absorption and sample shadowing at ω = 0° arises from the fact that the DAC has the lowest absorption for the primary beam entering the cell through the hole in the beryllium disc, and this absorption quickly increases when the ω angle is changed to about 5° and the primary beam enters the beryllium disc. However, this absorption effect is almost totally offset by the decreased shadowed sample volume at the low ζ angles.

Naturally, the changes of ω to angles different from 0° imply that the inclination of the reflected beams to the DAC axis (*i.e.* the ρ_r angles) becomes ζ-dependent. This dependence for the diffractometric ω positions described above are shown in Fig. 6. For low ζ angles, the inclination ρ_r is efficiently reduced, while, for ζ approaching 180°, ρ_r is unfavourably increased [compare equations (7) and (8)]. Most of the Merrill–Bassett DAC designs have a limiting access angle close to 40°, thus for the ω angle of 16° the reflection ring between 120 and 240°

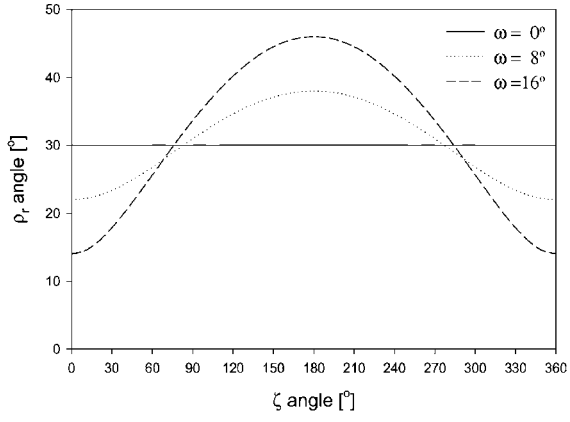

Figure 6
Dependence of the ρ_r angle between the DAC axis and the beams of the powder reflection ring diffracting at $2\theta_B$ = 30° as a function of the ζ angle (around the primary beam) for several inclinations of the DAC axis from the primary beam (measured by angle ω).

would be inaccessible due to the ρ_r angles exceeding the access limit.

The access to the sample and the shadowing effect become more drastic for higher 2θ-angle reflections: for the example illustrated in Fig. 7, the reflection at $2\theta = 50^\circ$ would be inaccessible for measurements at the $\omega = 0^\circ$ position, as all the ρ_r angles exceed the limiting angle. The reflection can be accessed by tilting the DAC, and in this case the tilting favourably reduces the combined effect of the DAC absorption and sample shadowing. The access to the sample can be gained for the ζ angle between -30 and 30° by tilting the cell to $\omega = 15^\circ$, and even to higher angles (see Fig. 8). At the same time, the shadowing effect is considerably reduced and this overcomes the increase of the DAC absorption outside the hole in the Be disc. Thus, for the $\theta = 25^\circ$ reflection, the DAC at $\omega = 0^\circ$ transmission is 0.739, the sample shadowing is 0.635 and the combined effect is 0.469; at $\omega = 15^\circ$, these values change to 0.684, 0.759 and 0.519; at $\omega = 20^\circ$ to 0.683, 0.775 and 0.529; and at $\omega = 25^\circ$ to 0.683, 0.783 and 0.535, respectively. In other words, at $\zeta = 0^\circ$, the combined effect of the reflection absorption and shadowing for the DAC positioned at $\omega = 25^\circ$ is by 14% smaller than at $\omega = 0^\circ$, and at the zero position the reflection would not be accessed at all due to the 40° opening of the DAC windows (see Fig. 8).

5. Specimen-related factors

The discussion above mainly relates to the instrument- and method- (mode of data collection) dependent factors. In high-pressure powder diffraction studies, there is also a number of factors affecting reflection intensities that are related to the specimen itself (McMahon, 2004). Some of these specimen-dependent factors are general for powder diffractometry – irrespective of the pressure attachments – like those of the sample absorption or extinction (Jenkins, 1989). There is also a number of sample-dependent factors that are particularly acute for high-pressure experiments with a DAC. These are preferred orientation and finite-particle-size effects. The volume of a high-pressure chamber is small, usually much smaller than 0.01 mm^3, and a limited number of sample particles can fit into it – even fewer particles fall into the volume illuminated by microbeams (with diameter of a few μm) applied at synchrotron sources. Moreover, some crystals tend to recrystallize into bigger particles when subjected to elevated pressures and temperatures, or when they undergo a reconstructive phase transition. Additionally, a non-hydrostatic strain generated in the high-pressure chamber along $\mathbf{x}_\varphi$ can produce a very significant preferred orientation of anisotropic crystal particles in the DAC. Both crystallite size and preferred orientation can considerably affect the intensity measurements and hamper the structural studies. The commonly applied remedy for these effects is rotation of the sample in the DAC when the diffraction image is being recorded. The larger the rotation, the more efficient are the smoothing of the particle-size effect and levelling of the preferred orientation. The rotations devised to counteract the particle-size effect can be taken about any direction, including the $\mathbf{x}_\varphi$ axis. However, the rotations about $\mathbf{x}_\varphi$ cannot average the effect of preferred orientation generated by the stress along this same direction $\mathbf{x}_\varphi$. Thus, to counteract the effect of preferred orientation generated in high-pressure cells, the diffraction data should be collected from the specimen positioned at various ω angles, and additionally at various ζ angles for a better statistical averaging if the grain-size effect is additionally present. Other specimen-dependent factors may be related to the residual strain or strain generated in the sample due to inhomogeneous pressure in the high-pressure chamber.

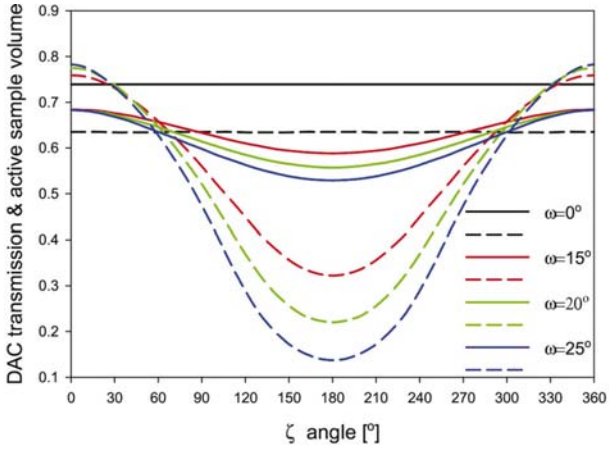

Figure 7
The ζ-angle dependence of the DAC relative transmission (solid lines) and the powder crystal sample volume actively contributing to the reflection (dashed lines) for powder ring reflection at Bragg angle 2θ equal to 25°.

6. Quadrature of numerical integration

Any numerical integration is bound to introduce quadrature errors if the integrated function is not uniform within the integration grid units (Krylov, 1967; Jankowska & Jankowski, 1981), which is a normal situation for the calculation of the absorption or shadowing effects. The quadrature equally

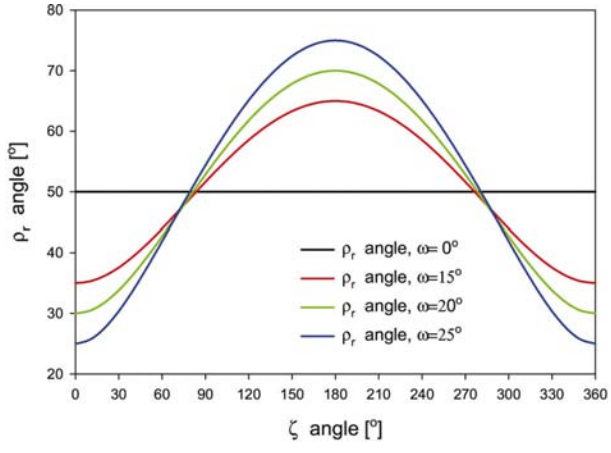

Figure 8
The ζ-angle dependence of ρ_r – the inclination between the primary beam and the beams of the powder reflection ring – for Bragg angle 2θ of 25°.

affects single-crystal (Katrusiak, 2004*b*) and powder diffraction corrections. The quadrature depends on many factors, such as the shape of the approximated function, size of the grid units and their orientation with respect to the functional directions. In the single-crystal studies, the shape of a given sample or of the high-pressure chamber is described in the φ-axis reference system, while the magnitudes of the absorption or shadowing corrections for a given reflection in most cases depend on the diffractometer setting angles (different ψ-angle positions). Thus, for the crystal samples with faces (other than spheres or specifically oriented cylindrically symmetric samples), the effects of quadrature can be evaluated by comparing analytically and numerically calculated corrections (Coppens *et al.*, 1967). In the case of powder diffraction reflections, the calculations of absorption and shadowing effects are calculated for a number of ζ segments of the reflection rings. When the DAC is oriented exactly along the x axis and the ideally cylindrical high-pressure chamber completely filled with the powdered sample, the effects of absorption and shadowing should be identical for all ring segments. Usually, the DAC absorption is calculated analytically and its magnitudes are identical for the identical ρ_r angles of the DAC aligned along **x**. However, the numerically evaluated shadowing changes slightly for different portions of the ring, as illustrated in Fig. 9. The errors have a clear structure depending on the applied grid, but it is also apparent that the denser grids systematically decrease the calculated active sample volume. The pattern of the distortions in the shadowing function clearly depends on the orientation of the φ-axis reference system and on the chosen numerical procedures. In the performed calculations (Katrusiak, 2004*b*), the quadrature effects are symmetrical with respect to **y** and **z** (*i.e.* along the directions corresponding to 0 and 90° ζ-angle values, respectively); owing to the convex shape of the approximated shape, the calculated active volume decreases with denser grid. The $10 \times 40 \times 40$ grid applied in the calculations presented above are overestimated by approximately 0.6%. The $40 \times 120 \times 120$ grid (576000 grid points for each of the powder reflection ring ζ sectors) produces a slightly fluctuating curve, with lower values at ζ equal to 0 or 90° (where the rectangular integration-grid-unit edges are approximately parallel to the cylinder wall) than for ζ equal to 45 or 135° (where the cylinder wall lies approximately along the diagonals of the units). The grid size should be adjusted to the divisions of the reflection rings into sectors of the ζ angle (see Figs. 1 and 2). It appears that the quadrature errors induced by the $10 \times 40 \times 40$ grid numeration are insignificant compared with the errors induced by the irregularities and precision of the measurement of the high-pressure-chamber dimensions, or other effects like inhomogeneity of the primary beam, extinction in the sample, particle size and preferred orientation, multiple reflections or simultaneous diffraction events from the diamond anvils. Owing to the small mosaic spread in diamond and high divergence of the incident graphite-monochromated beams, the simultaneous-reflection events from the anvils insignificantly affect the intensity of small sectors of the reflections when the DAC axis is rotated away from the primary beam – moreover, the orientation of the anvils can be determined from the recorded images and the affected ring sectors identified and corrected or excluded.

7. Experimental

For experimentally measuring the effect of shadowing of the sample powder crystal by gasket edges, an NaCl crystal and a gasket of 0.2 mm Inconel foil were chosen. The gasket was mounted on one anvil of a DAC, and the chamber was filled with the NaCl powder with some excess. Then this excess was pressed into the chamber by gently squeezing the gasket with the opposite anvils. After opening the DAC, the gasket was removed. The NaCl powder fully filled the hole in the gasket, forming a cylindrical pellet, 0.3 mm in diameter and 0.195 mm high, with flat pellet bases aligned along the gasket surfaces.

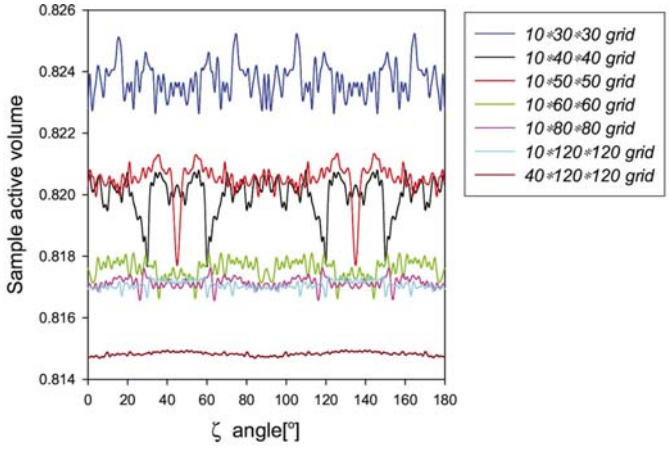

Figure 9
Sample active volume calculated for a cylindrical high-pressure chamber by numerical integration with several grid divisions listed in the legend (along the chamber height, **x**, and two diagonal directions **y** and **z**, respectively).

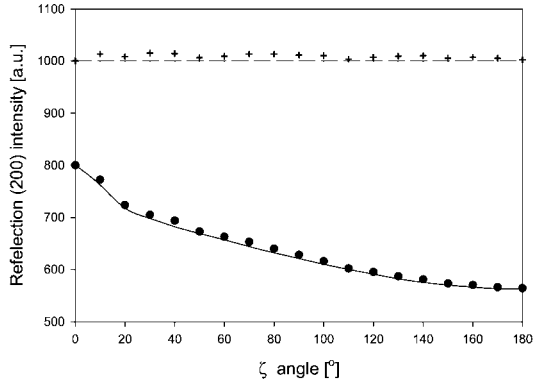

Figure 10
The intensity of reflection 200 from the NaCl powder pellet 0.3 mm in diameter and 0.195 mm high tightly filling the hole in the Inconel gasket, as a function of angle ζ (black circles), rescaled to the sample volume actively contributing to the reflection intensity. The gasket is inclined by $\omega = 30°$ to the incident beam. The dashed line shows the ideally corrected theoretical intensity calculated from the actively scattering sample volume and the crosses show the corrected measured intensities.

The gasket with the pellet was centred on a KM-4 Kuma four-circle diffractometer. Graphite-monochromated Cu $K\alpha$ sealed-tube radiation and a 0.5 mm collimator were applied. Then the I_{200} reflection was centred with the goniometer angles set at 0° (gasket perpendicular to the primary beam) at $2\theta_{200} = 31.71°$, after which the gasket was rotated to $\varphi_e = 30°$, the χ angle was changed in 10° steps between −90 and 90° and the reflection intensity and its background at each step were measured. The experiment has been described in the Eulerian geometry here, hence the 'e' subscript; the κ angles were set at appropriate positions to produce the required Eulerian setting, *e.g.* each step in χ with constant φ_e involved simultaneous changes of φ_κ, κ and ω_κ (subscript 'κ' indicates κ-geometry angles, *i.e.* the goniometer angles in this experiment). The I_{200} intensity as a function of angle ζ along the reflection ring is plotted in Fig. 10.

It is apparent that the shadowing of the sample by the gasket edges affects the detected intensity and that it is corrected according to the sample volume actively contributing to the reflection (see Fig. 10). Systematically, somewhat higher experimental measurements (circles and crosses) than the theoretical ones (lines) can be attributed to some small transmission of X-rays through the gasket material and to small rounding of the hole edges close to the gasket surface, while the ideally cylindrical hole was assumed for the calculations.

8. Conclusions

The presented means of correcting shadowing and absorption effects for a DAC is relatively simple and can be applied to any techniques of high-pressure powder diffraction, either angle- or energy-dispersive (Brister, 1992), and to any type of detector geometry. The corrections are described in the φ-axis reference systems of a four-circle diffractometer, which was aimed at using a laboratory diffractometer equipped with a CCD detector (Paciorek *et al.*, 1999) for preliminary high-pressure powder diffraction studies. The described absorption and shadowing corrections, apart from increasing the accuracy of the measured intensities of reflections, can be used for removing experimental constraints, such as a requirement that the DAC axis be aligned along the primary beam. Unrestricted positioning of the DAC can be used for eliminating other undesired effects notorious in high-pressure powder diffraction experiments – particle size and preferred orientation – and for optimally planning data-collection modes for high-pressure experiments with respect to the DAC absorption and completeness of the data (Takata & Sakata, 1996). This improved accuracy of single-crystal diffraction data allows pressure-crystallized structures to be solved by direct methods and refined to a good accuracy routinely in our laboratory. It is hoped that the progress in experimental and computational techniques related to high-pressure studies will soon allow electron density to be determined either by single-crystal or powder techniques at laboratory and synchrotron sources.

References

Adler, P., Schwarz, U., Syassen, K., Rozenberg, G. Kh., Machavariani, G. Yu., Milner, A. P., Pasternak, M. P. & Hanfland, M. (1999). *Phys. Rev. B*, **60**, 4609–4617.

Akahama, Y., Kawamura, H., Haeuserman, D., Hanfland, M. & Shimomura, O. (1995). *Phys. Rev. Lett.* **74**, 4690–4693.

Allan, D. A., Clark, S. J., Dawson, A., McGregor, P. A. & Parsons, S. (2002). *Acta Cryst.* B**58**, 1018–1024.

Baer, B. J., Cynn, H., Iota, V. & Yoo, Ch.-Sh. (2003). *Phys. Rev. B*, **67**, 134115-1–7.

Brister, K. (1992). *Rev. Sci. Instrum.* **61**, 995–998.

Budzianowski, A. & Katrusiak, A. (2004). *High-Pressure Crystallography*, edited by A. Katrusiak & P. F. McMillan, pp. 101–112. Dordrecht: Kluwer Academic Publishers.

Bujak, M., Budzianowski, A. & Katrusiak, A. (2004). *Z. Kristallogr.* In the press.

Burnham, Ch. W. (1966). *Am. Mineral.* **51**, 159–167.

Busing, W. R. & Levy, H. A. (1957). *Acta Cryst.* **10**, 180–182.

Chacham, H., Zhu, X. & Louie, S. G. (1992). *Phys. Rev. B*, **46**, 6688–6699.

Chall, M., Knorr, K., Ehm, L. & Depmeir, W. (2000). *High Press. Res.* **17**, 315–323.

Coppens, P., Cox, D., Vlieg, E. & Robinson, I. K. (1992). *Synchrotron Radiation Crystallography*. London: Academic Press.

Coppens, P., de Meulenaer, J. & Tompa, H. (1967). *Acta Cryst.* **22**, 601–602.

Crichton, W. A. & Mezouar, Z. (2004). *High-Pressure Crystallography*, edited by A. Katrusiak & P. F. McMillan, pp. 113–130. Dordrecht: Kluwer Academic Publishers.

Dinnebier, R. E., Olbrich, F., van Smaalen, S. & Stephens, P. W. (1997). *Acta Cryst.* B**53**, 153–158.

Edwards, P. P. & Hensel, F. (1997). *Nature (London)*, **388**, 621–622.

Eremets, M. I., Gregoryanz, E. A., Struzhkin, V. V., Mao, H.-K. & Hemley, R. J. (2000). *Phys. Rev. Lett.* **85**, 2797–2800.

Eremets, M. I., Hemley, R. J., Mao, H.-K. & Gregoryanz, E. (2001). *Nature (London)*, **411**, 170–174.

Fiquet, G. & Andrault, D. (1999). *J. Synchrotron Rad.* **6**, 81–86.

Fujii, Y., Hose, K., Ohishi, Y., Fujihisa, H., Hamaya, N., Takemura, K. & Shimomura, O. (1989). *Phys. Rev. Lett.* **63**, 536.

Goncharov, A. F., Gregoryanz, E., Mao, H.-K., Liu, Z. & Hemley, R. J. (2000). *Phys. Rev. Lett.* **85**, 1262–1265.

Hazen, R. M. & Finger, L. W. (1982). *Comparative Crystal Chemistry*. New York: John Wiley.

Hemley, R. J. (1998). *Science*, **281**, 1296–1297.

Jankowska, J. & Jankowski, M. (1981). *Przegląd Metod i Algorytmów Numerycznych.*, Vol. 1, pp. 127–166. Warsaw: Wydawnictwo Naukowo-Techniczne. (In Polish.)

Jenkins, R. (1989). *Modern Powder Diffraction. Rev. Mineral.* **20**, 19–45, 47–71.

Katrusiak, A. (2001). *Z. Kristallogr.* **216**, 646–647.

Katrusiak, A. (2004*a*). *High-Pressure Crystallography*, edited by A. Katrusiak & P. F. McMillan, pp. 57–68. Dordrecht: Kluwer Academic Publishers.

Katrusiak, A. (2004*b*). *Z. Kristallogr.* **219**, 461–467.

Katrusiak, A. & Ryan, T. (1988). *Acta Cryst.* A**44**, 623–627.

Kikegawa, T. & Iwasaki, H. (1983). *Acta Cryst.* B**39**, 158–164.

Krylov, V. I. (1967). *Priblizhennoe Vychiclene Integralov*, 2nd ed. Moscow: Nauka. (In Russian.)

McMahon, M. I. (2004). *High-Pressure Crystallography*, edited by A. Katrusiak & P. F. McMillan, pp. 1–20. Dordrecht: Kluwer Academic Publishers.

Meade, C. & Jeanloz, R. (1990). *Rev. Sci. Instrum.* **61**, 2571–2580.

Merrill, L. & Bassett, W. A. (1974). *Rev. Sci. Instrum.* **45**, 290–294.

Mesot, J., Medarde, M., Rosenkranz, S., Fisher, P., Lacorre, P. & Gobrecht, K. (1995). *High Press. Res.* **14**, 35–40.

Neaton, J. B. & Ashcroft, N. W. (1999). *Nature (London)*, **400**, 141–144.

Nelmes, R. J., Hatton, P. D., McMahon, M. I., Piltz, R. O., Crain, J., Cernik, R. J. & Dushnell-Wye, G. (1992). *Rev. Sci. Instrum.* **63**, 1039–1042.
Nicol, M. & Yin, G. Z. (1981). *J. Phys. (Paris) Colloq. 8*, **48**, 163–172.
Paciorek, W. A., Meyer, M. & Chapuis, G. (1999). *Acta Cryst.* A**55**, 543–557.
Parise, J. B. (2004). *High-Pressure Crystallography*, edited by A. Katrusiak & P. F. McMillan, pp. 37–56. Dordrecht: Kluwer Academic Publishers.
Piltz, R. O., McMahon, M. I., Crain, J., Hatton, P. D., Nelmes, R. J., Cernik, R. J. & Bushnell-Wye, G. (1992). *Rev. Sci. Instrum.* **63**, 700–703.
Prewitt, C. T., Coppens, P., Phillips, J. C. & Finger, L. W. (1987). *Science*, **238**, 312–318.
Serra, S., Chiarotti, G., Scandolo, S. & Tosatti, E. (1998). *Phys. Rev. Lett.* **80**, 5160–5163.
Shimizu, K., Suhara, K., Ikumo, M., Eremets, M. I. & Amaya, K. (1998). *Nature (London)*, **393**, 767–768.
Shimomura, O., Takemura, K., Fujihisa, H., Fujii, Y., Ohishi, Y., Kikegawa, T., Amemiya, Y. & Matsushita, T. (1992). *Rev. Sci. Instrum.* **63**, 967–972.
Shobu, T., Noda, Y., Iwasa, K., Hannan, A., Koghi, M., Ishimatsu, N. & Shimomura, O. (2001). *J. Phys. Soc. Jpn*, **70**, 1162–1163.
Siringo, F., Pucci, R. & March, N. H. (1990). *High Press. Res.* **2**, 109–134.
Struzhkin, V. V., Hemley, R. J., Mao, H.-K. & Timofeev, Yu. A. (1997). *Nature (London)*, **370**, 678.
Takata, M. & Sakata, M. (1996). *Acta Cryst.* A**52**, 287–290.
Von Dreele, R. B. (1999). *J. Appl. Cryst.* **32**, 1084–1089.
Von Dreele, R. B. (2001). *Acta Cryst.* D**57**, 1836–1842.
Von Dreele, R. B. & Hanson, R. C. (1984). *Acta Cryst.* C**40**, 1635–1638.
Von Dreele, R. B., Stephens, P. W., Smith, G. D. & Blessing, R. H. (2000). *Acta Cryst.* D**56**, 1549–1553.
Yin, M. T. & Cohen, M. L. (1983). *Phys. Rev. Lett.* **50**, 1172.
Yoder-Short, D. R., Colella, R. & Weinstein, B. A. (1982). *Phys. Rev. Lett.* **49**, 1438–1441.